Finite Element Prediction of Sheet Forming Defects Using Elastic-Plastic, Damage and Localization Models

Badis Haddag, Farid Abed-Meraim and Tudor Balan

LPMM, UMR7554, ENSAM Metz, 4 rue A. Fresnel, 57078 Metz Cedex 3, France

Abstract. In this work, an advanced anisotropic elastic-plasticity model is combined with a damage model and a strain localization criterion in the aim to describe accurately the mechanical behavior of sheet metals. Large strain, fully three-dimensional, implicit time integration algorithms are developed for this model and implemented in the finite element code Abaqus. The resulting code is used to predict the strain localization limits as well as the springback after forming of sheet steels. The impact of strain-path dependent hardening models on the limit strains and on the amount of springback is addressed.

Keywords: elastic-plasticity, strain-path-dependent hardening, damage, large strains, implicit time integration, sheet metal forming, springback, forming limits, finite element simulation.
PACS:

INTRODUCTION

Finite element simulations are widely used in the setup of new sheet forming processes. The prediction of forming defects like strain localization and springback are some of the current challenges in this research field. The accuracy of such predictions depends on several factors. In this work, the effort is concentrated on a rich and complete constitutive modeling. An anisotropic, elastic-plastic strain-path dependent hardening model [1] is coupled to a scalar damage model [2]. The strain localization criterion of Rice [3] has been selected for its rigorous mathematical background. The numerical implementation of the resulting models has been carried out using an implicit time integration scheme [4].

ELASTIC-PLASTIC CONSTITUTIVE MODEL

When rotation-compensated tensor variables are considered, the hypo-elastic law takes the simple form:

$$\dot{\boldsymbol{\sigma}} = \mathbf{C} : \mathbf{D}^{e} = \mathbf{C} : \left(\mathbf{D} - \mathbf{D}^{p} \right) \qquad (1)$$

where $\mathbf{C}$ is the fourth order tensor of the elastic constants, while $\mathbf{D}$ and $\mathbf{D}^{e}$ are the strain rate and elastic strain rate tensors, respectively. The plastic strain rate tensor $\mathbf{D}^{p}$ is given by the associated flow rule:

$$\mathbf{D}^{p} = \dot{\lambda} \frac{\partial F}{\partial \boldsymbol{\sigma}} = \dot{\lambda} \mathbf{V} \qquad (2)$$

where $\mathbf{V}$ is the flow direction normal to the yield surface defined by the potential F, and $\dot{\lambda}$ is the plastic multiplier to be determined from the loading-unloading criterion:

$$F = \bar{\sigma}(\mathbf{T}) - Y \leq 0, \quad \mathbf{T} = \boldsymbol{\sigma}' - \mathbf{X} \qquad (3)$$

where $\bar{\sigma}$ is the equivalent stress, a function of $\boldsymbol{\sigma}'$ (the deviatoric part of the Cauchy stress) and the back-stress $\mathbf{X}$, whereas Y is the size of the yield surface.

If hardening is governed by rate equations of the form:

$$\dot{Y} = H_{Y} \dot{\lambda}, \qquad \dot{\mathbf{X}} = \mathbf{H}_{\mathrm{X}} \dot{\lambda} \qquad (4)$$

the consistency condition $\dot{F} = 0$ combined with the previous equations lead to the following expression of the tangent elastic-plastic modulus:

$$\mathbf{C}^{ep} = \mathbf{C} - \alpha \frac{(\mathbf{C} : \mathbf{V}) \otimes (\mathbf{V} : \mathbf{C})}{\mathbf{V} : \mathbf{C} : \mathbf{V} + \mathbf{V} : \mathbf{H}_{\mathrm{X}} + H_{Y}} \qquad (5)$$

So far, the material model has been kept in a general analytical form. The yield function is defined by the equivalent stress $\bar{\sigma}$ and its gradient **V,** while the hardening is defined by H_{Y} and $\mathbf{H}_{\mathrm{X}}$.

Hardening model

A macroscopic hardening model with a sound microstructural background has been proposed by Teodosiu and co-workers [5,6]. The isotropic hardening is governed by a saturating law of the form:

$$\dot{R} = C_R \left(R_{sat} - R \right) \dot{\lambda} = H_R \dot{\lambda} \qquad (6)$$

where C_R characterizes the saturation rate of the scalar variable R and R_{sat} is its saturation value. The kinematic hardening is governed by the equation:

$$\dot{\mathbf{X}} = C_X \left(X_{sat} \mathbf{n} - \mathbf{X} \right) \dot{\lambda} = \mathbf{H}_\mathbf{X} \dot{\lambda} \qquad (7)$$

where C_X is a material parameters characterizing the saturation rate of $\mathbf{X}$, while $\mathbf{n} = (\boldsymbol{\sigma}' - \mathbf{X}) / \bar{\sigma}$ is the saturation direction. X_{sat} is no longer a constant (like in more classical models) but a function of the new internal variables **S** (fourth order tensor) and **P** (second order tensor). The variable ***S*** is further decomposed in two parts: a scalar, "active" part S_D=**N**:**S**:**N** and a tensorial, "latent" part $\mathbf{S}_L$=**S**-S_D**N**⊗**N**. Saturating rate equations are postulated for all these variables:

$$\dot{S}_D = C_{SD} [g(S_{sat} - S_D) - h S_D] \dot{\lambda} = H_{SD} \dot{\lambda} \qquad (8)$$

$$\dot{\mathbf{S}}_L = -C_{SL} (|\mathbf{S}_L| / S_{sat})^n \mathbf{S}_L \dot{\lambda} = \mathbf{H}_{SL} \dot{\lambda} \qquad (9)$$

$$\dot{\mathbf{P}} = C_P (\mathbf{N} - \mathbf{P}) \dot{\lambda} \qquad (10)$$

New material parameters are introduced: C_{SD}, C_{SL}, C_P, S_{sat}, n, while g and h are functions of the internal variables. The size of the yield surface is given by $Y = Y_0 + R + f\,|\mathbf{S}|$ where f is also a material parameter. More details can be found in the original papers. We shall simply note here that this model can be rearranged in the generic form (4), with:

$$H_Y = \frac{f}{|\mathbf{S}|} \left(S_D H_{SD} - |\mathbf{S}_L| |\mathbf{H}_{SL}| \right) + H_R \qquad (11)$$

TIME INTEGRATION ALGORITHM

The FE implementation of such a model requires the numerical integration of these equations over a time increment, from a known state at time t_n to the unknown state at t_{n+1} – given the total strain increment $\Delta\boldsymbol{\varepsilon}$. The most widely used method is the fully implicit, backward Euler integration scheme [7,8,9]. This method leads to the following discrete form of the constitutive equations (1)-(4):

$$\Delta\boldsymbol{\sigma} = \mathbf{C} : \left(\Delta\boldsymbol{\varepsilon} - \Delta\boldsymbol{\varepsilon}^p \right) \qquad (12)$$

$$\Delta\boldsymbol{\varepsilon}^p = \Delta\lambda \mathbf{V}_{n+1} \qquad (13)$$

$$F_{n+1} = \bar{\sigma} \left(\mathbf{T}_{n+1} \right) - Y \left(\mathbf{y}_{n+1} \right) = 0 \qquad (14)$$

$$\Delta\mathbf{y} = \mathbf{h}_1 (\mathbf{y}_{n+1}, \boldsymbol{\sigma}_{n+1}, \Delta\lambda) \qquad (15)$$

The major inconvenient here is that the number of equations increases with the number of internal variables, thus inducing large computing times and possibly numerical difficulties for complex constitutive laws. Nevertheless, the particular structure of the hardening models and the physical properties of the internal variables allow in most cases for explicit update equations in the following form:

$$\mathbf{y}_{n+1} = \mathbf{h}_2 (\mathbf{T}_{n+1}, \Delta\lambda) \qquad (16)$$

In this case, the nonlinear set of equations (12)-(15) can be reduced to the resolution of the following system of six scalar equations:

$$\mathbf{T}_{n+1} - \boldsymbol{\sigma}'_n - \mathbf{C} : \Delta\boldsymbol{\varepsilon}' + \mathbf{C} : \mathbf{V} \left(\mathbf{T}_{n+1} \right) \Delta\lambda + \mathbf{X} \left(\mathbf{T}_{n+1}, \Delta\lambda \right) = \mathbf{0} \qquad (17)$$

$$F_{n+1} = \bar{\sigma} \left(\mathbf{T}_{n+1} \right) - Y \left(\mathbf{y}_{n+1} \left(\mathbf{T}_{n+1}, \Delta\lambda \right) \right) = 0 \qquad (18)$$

The size of this system is independent of the hardening model and thus allows for a robust and effective resolution. The internal variables are then updated using equation (18), derived by means of the backward Euler or semi-analytical formulas. In order to preserve the quadratic convergence rate, the tangent modulus consistent with the resulting state update algorithm has been derived [4].

APPLICATION TO SPRINGBACK SIMULATION

The strip drawing test is regularly used to address springback is sheet metal forming. Two-dimensional simulations have been performed here using four layers of linear solid elements with selective reduced integration (figure 1). During this test, typical strain reversal (bending – unbending) occurs in the external layers of the sheet. Consequently, kinematic hardening is expected to play a crucial role in the prediction of springback. However, it has been often reported in literature [10] that most hardening models predict very similar springback angles. This is confirmed by the results in figure 2, where the extreme cases of purely isotropic and purely kinematic hardening are compared.

This reduced sensitivity to the hardening model may be related to the low levels of pre-strain induced during bending on the die radius. In order to verify this hypothesis, a second test geometry has been considered where the die radius is smaller, so that the pre-strains are increased more than three times during the bending step. As shown in figure 3, the hardening model has a much more important effect in this case. The Teodosiu-Hu model is compared to the classical isotropic-kinematic hardening model of Chaboche (equations (6)-(7) with X_{sat} constant).

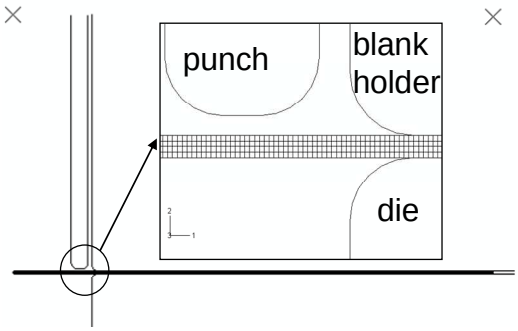

FIGURE 1. Strip drawing test: tools and finite element mesh (detail).

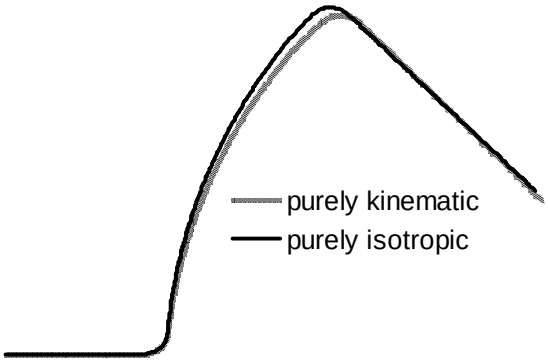

FIGURE 2. Springback predictions for a typical strip drawing test, using purely isotropic / kinematic hardening models.

As a conclusion, the strain-path dependent hardening models may have an important role in the accurate simulation of sheet forming processes where abrupt strain-path changes may occur after relevant pre-strains.

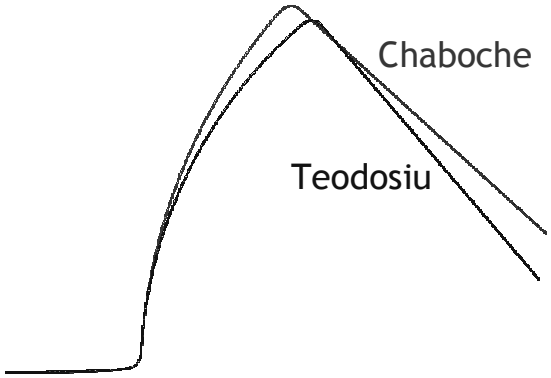

FIGURE 3. Springback predictions for a strip drawing test with smaller tool radii, using combined isotropic-kinematic hardening models.

MODELING OF STRAIN LOCALIZATION AND DAMAGE

Strain localization and damage are two important phenomena that may occur when large strains are attained in sheet metal forming. In macroscopic approaches, damage is often described as a state variable in the context of continuum damage mechanics [2]. Here, a scalar damage variable d is considered that allows for the definition of an effective stress as:

$$\tilde{\boldsymbol{\sigma}} = \frac{\boldsymbol{\sigma}}{1-d} \qquad (19)$$

The effective stress enters the expression of the yield criterion (20), flow rule (21), hardening laws etc.

$$F = \bar{\tilde{\sigma}}(\tilde{\boldsymbol{\sigma}}' - \mathbf{X}) - Y \le 0 \qquad (20)$$

$$\mathbf{D}^p = \dot{\lambda}\frac{\partial F}{\partial \boldsymbol{\sigma}} = \dot{\lambda}\tilde{\mathbf{V}},\ \tilde{\mathbf{V}} = \frac{1}{1-d}\mathbf{V} \qquad (21)$$

The time evolution of the damage variable has been considered in the following form:

$$\dot{d} = \frac{1}{(1-d)^{\beta}}\left(\frac{\langle Y_e - Y_{ei}\rangle}{S}\right)^{s}\dot{\lambda} = H_d\dot{\lambda} \qquad (22)$$

with

$$Y_e = \frac{J_2^2}{2(1-d)^2 E}\left[\frac{2}{3}(1+\nu)+3(1-2\nu)\left(\frac{\sigma^s}{J_2}\right)^2\right] \qquad (23)$$

where σ^s is the spherical part of the stress tensor, E and ν are the Young modulus and Poisson coefficient. The tangent modulus for the damage-affected elastic-plastic model is then derived as:

$$\mathbf{C}^{Ana} = \tilde{\mathbf{C}} - \alpha\left(\frac{(\mathbf{C}:\mathbf{V})\otimes(\mathbf{V}:\mathbf{C})}{H_\lambda} + \frac{H_d\tilde{\boldsymbol{\sigma}}\otimes(\mathbf{V}:\mathbf{C})}{H_\lambda}\right) \qquad (24)$$

where $H_\lambda = \mathbf{V}:\mathbf{C}:\tilde{\mathbf{V}} + \mathbf{V}:\mathbf{H}_X + H_Y$ and $\tilde{\mathbf{C}} = (1-d)\mathbf{C}$.

For the detection of strain localization, the criterion (25) of Rudnicki and Rice [3] is considered, where $\boldsymbol{L}$ is the modulus relating the rate of nominal stress $\mathbf{N}$ to the velocity gradient $\mathbf{G}$ (26).

$$\det(\mathbf{n}\cdot\boldsymbol{L}\cdot\mathbf{n}) = 0 \qquad (25)$$

$$\dot{\mathbf{N}} = \boldsymbol{L}:\mathbf{G};\quad \boldsymbol{L} = \mathbf{L} + \mathbf{L}_1 - \mathbf{L}_2 - \mathbf{L}_3 \qquad (26)$$

where $L_{1ijkl} = \sigma_{ij}\delta_{kl}$, $L_{2ijkl} = \frac{1}{2}\left[\delta_{ik}\sigma_{lj} + \delta_{il}\sigma_{kj}\right]$ and $L_{3ijkl} = \frac{1}{2}\left[\sigma_{ik}\delta_{lj} - \sigma_{il}\delta_{jk}\right]$.

In equation (25), the normal $\mathbf{n}$ is numerically searched-for in the whole space of possible directions, at every time step and at every integration point. In equation (26), $\boldsymbol{L}=\boldsymbol{C}^{Ana}$ is the small-strain analytical tangent modulus given by equation (24).

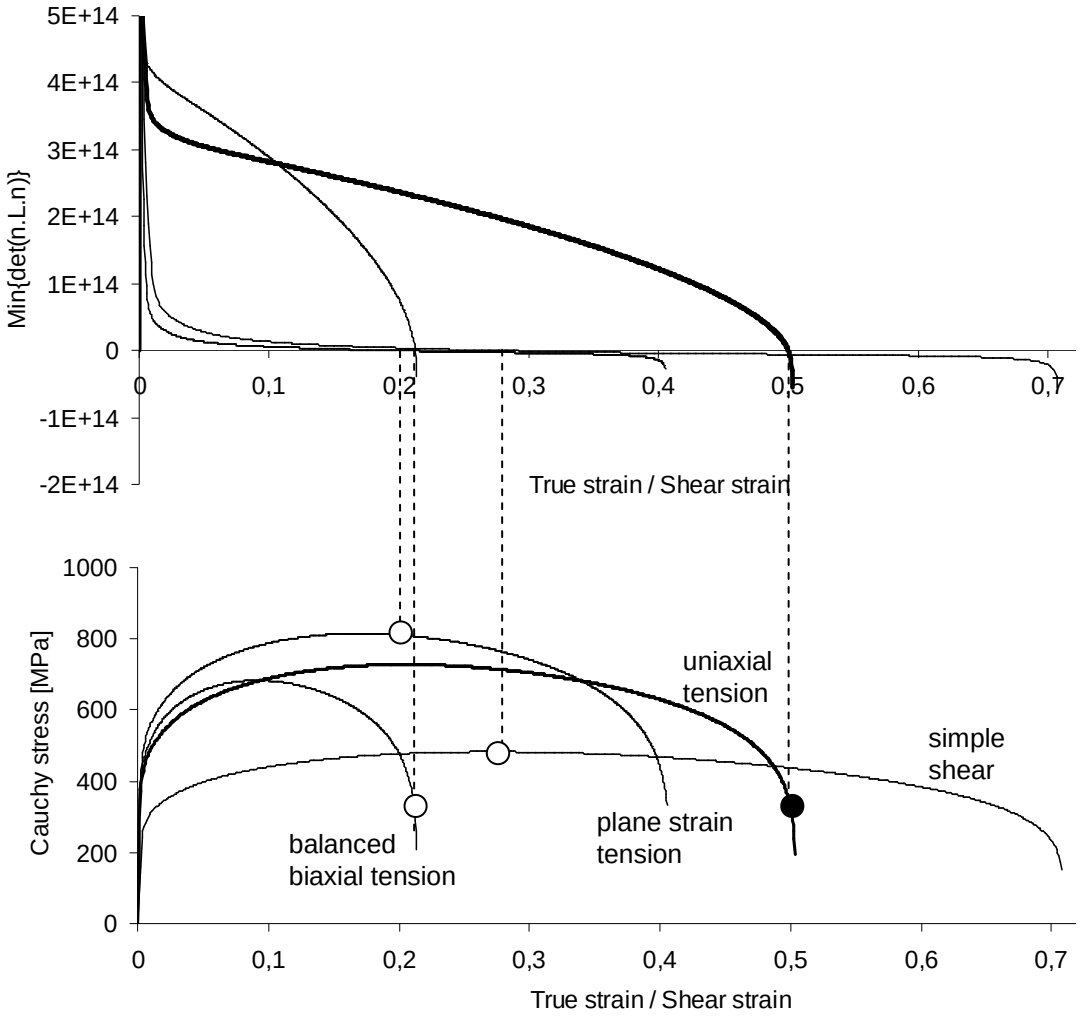

FIGURE 4. Loading paths simulation (bottom) and detection of strain localization with Rice's criterion (top).

FORMING LIMIT DIAGRAM PREDICTION

The strain localization criterion (25), coupled to the damage-affected elastic-plastic model, has been applied to predict the limit strains during simple loading paths. Figure 4 shows the resulting stress-strain curves as well as the evolution of the localization criterion.

The limits strains are plotted in figure 5 for different sets of arbitrary damage parameters. A strong dependency of the FLD to the damage model parameters is observed, requiring for careful parameter identification.

The strain-path dependency of the forming limit strains has been investigated. Two pre-straining modes have been considered, in uniaxial tension and balanced biaxial tension. As shown in figure 6, the well-known shift of the FLD in the direction of the pre-strain is well described by the considered criterion. The stress-strains corresponding to the uniaxial tensile prestrains are plotted in figure 7. The transient zones after strain-path changes are well reproduced by the Teodosiu-Hu model and their effect is combined to the damage one.

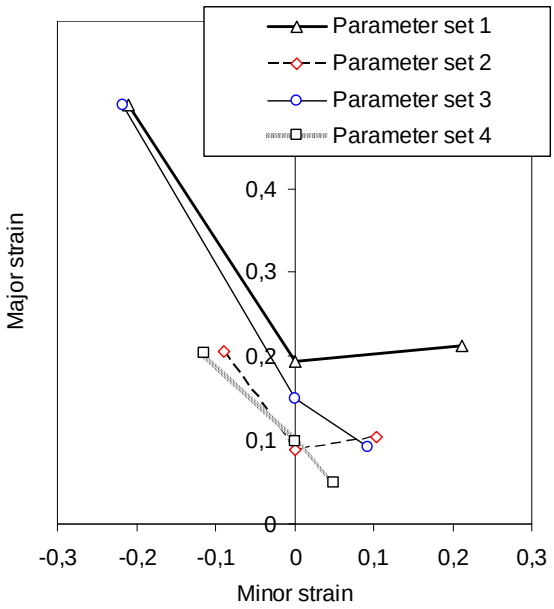

FIGURE 5. FLD predicted with Rice's criterion and different parameters of the damage law.

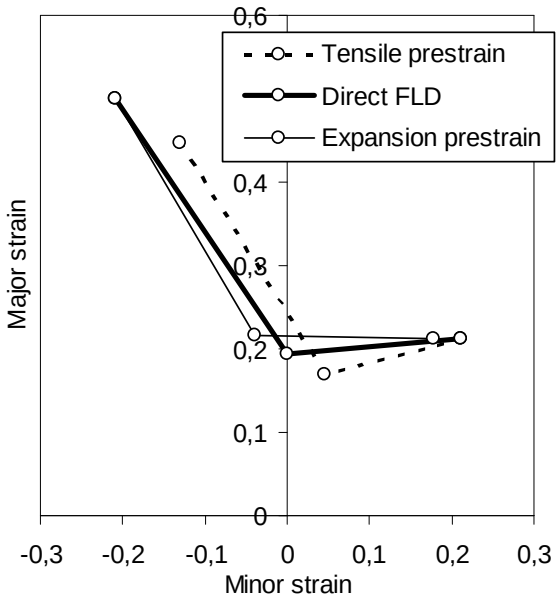

FIGURE 6. Effect of strain-path changes on the FLD (parameter se no. 1).

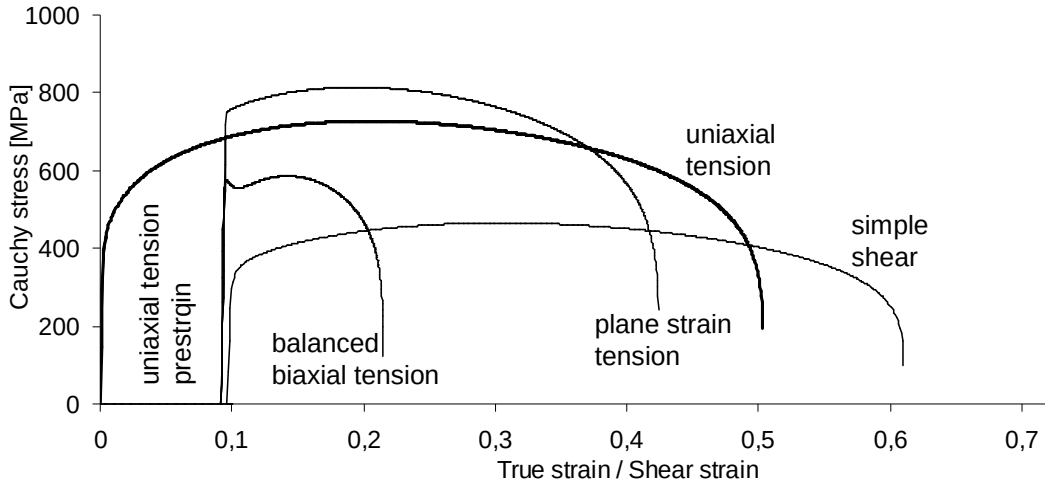

FIGURE 7. Different loading paths simulations after a uniaxial tensile prestrain.

CONCLUSIONS

The aim of this work was to describe and study the steel sheet behaviour during forming operations. The applications in mind concern the prediction, through the forming process numerical simulation, of major defects like springback and strain localization. The microstructural work-hardening model of Teodosiu-Hu has been considered to take into account transient work-hardening due to the strain-path changes. This model has been improved, by coupling with the Lemaitre-Chaboche damage model, in order to reproduce the softening that appears prior to failure. In addition, Rice's localisation criterion by shear bands has been introduced and written in the large strain framework. The developed modelling takes into account the initial plastic anisotropy, the work-hardening-induced anisotropy, the damage and finally strain localisation.

A robust and efficient computer implementation has been performed in a finite element code, in order to apply the developed models to forming process simulation. Direct and sequential rheological tests have been simulated in order to validate the computer implementation, with very good results. The application of the elastic-plastic model to a springback analysis highlighted the impact of advanced hardening

models, like the Teodosiu-Hu one. Eventually, a strain localisation analysis has been performed using Rice's criterion and the elastic-plastic model coupled to damage. This study showed the capability of this approach to predict the forming limit diagrams during direct and two-step loading paths.

ACKNOWLEDGMENTS

The financial support from Arcelor Research is gratefully acknowledged.

REFERENCES

1. H. Haddadi, S., Bouvier, M., Banu, C., Maier and C., Teodosiu, Int. J. Plasticity, **22**, 2226-2271 (2006).
2. J.L. Chaboche. Thermodynamically founded CDM models for creep and other conditions: CISM Courses and lectures No.399, International Centre for Mechanical Sciences. Creep and Damage in Materials and structures, 209-283, 1999.
3. J.W. Rudnicki and J.R. Rice, J. Mech. Phys. Solids **23**, 371–394 (1975).
4. B. Haddag, T. Balan, F. Abed-Meraim, "Investigation of advanced strain-path dependent material models for sheet metal forming simulations", Int. J. Plasticity, in press.
5. Teodosiu, C., Hu, Z., "Evolution of the intragranular microstructure at moderate and large strains: Modelling and computational significance" in *Simulation of Materials Processing: Theory, Methods and Applications*, Numiform'95 Proceedings, 1995, pp. 173-182.
6. Teodosiu, C., Hu, Z., "Microstructure in the continuum modelling of plastic anisotropy" in *The 19th Riso Int. Symp. On Materials Science Proceedings*, Roskilde, 1998, pp. 149-168.
7. T.J.R. Hughes, "Numerical implementation of constitutive models: rate-independent deviatoric plasticity" in *Theoretical foundation for large-scale computations for nonlinear material behavior*, Netherlands: Martinus Nij Publishers, 1984, pp. 29-57.
8. J. Simo, R., Taylor, Comp. Meth. Appl. Mech. Engng. **48**, 101-118, 1985.
9. M. Ortiz, E.P. Popov, Int. J. Num. Methods Engng. **21**, 1561-1576 (1985).
10. Bouvier, S., Alves, J.L., Oliveira, M.C., Menezes, L.F., Comp. Mater. Sci. **32**, 301-315., 2005.